Fuel,Volume 253, October 2019, pp. 1204-1213
DOI: 10.1016/j.fuel.2019.05.077

Deposition prediction in a pilot scale pulverized fuel-fired combustor

C. Riccio, N.J. Simms*, J.E. Oakey
Cranfield University, Cranfield Bedfordshire, UK, MK43 0AL

*Corresponding author:
email: n.j.simms@cranfield.ac.uk
Tel: +44 (0)1234 752954

Highlights:

- CFD model developed for ash and vapour deposition onto heat exchanger tubes
- Pilot scale co-firing experiments conducted with 12 wt.% Miscanthus - Daw Mill Coal
- CFD model applied using experimental boundary conditions and ash size distributions
- Predictions and experimental data for deposition fluxes, shapes and temperatures

Abstract

Fossil fuels have traditionally been used in power generation systems and represent the main source of greenhouse gas emissions from this sector. Renewable fuels, especially biomass, are now being substituted for fossil fuels to reduce CO_2 emissions. Co-firing biomass with coal, which has been widely practised in the UK and Europe, is one route to reduce the environmental impact of using coal. However, the deposition of ash particles and vapour species on heat exchanger surfaces during operation is a serious issue in pulverised coal and biomass fired power plant as this reduces the plant thermal efficiency and can cause fireside corrosion, which limits component lives. Deposit formation is difficult to predict as it varies with many factors including: boiler geometry, combustion conditions and fuel composition.

Computational Fluid Dynamics (i.e. CFD) is one of the best modelling tools to study the flow behaviour of gases and particles around heat exchanger tubes and predict deposition. This work used an Eulerian-Lagrangian model to describe the gas flow field around tubes and the solid ash particle trajectories respectively. User Defined Functions (i.e. UDFs) were developed for the CFD package to enable the prediction of deposit growth, deposit shape and temperature gradients around superheater/reheater tubes. Deposit build up insulates such tubes from the flow of the hot combusted gas stream and reduces heat transfer between this gas stream and the steam coolant following within the tubes, thus raising the deposit temperature. The CFD-based predictions generated were consistent with available literature data.

The CFD deposition model has been applied to predict deposition on air cooled ceramic probes in a 100 kWth pilot-scale, pulverized fuel (PF) combustor and compared to deposition data measured after the combustor rig runs. For modelling purposes, the geometry was simplified to a two-dimensional domain with inert spherical ash particles dispersed in air and injected at an inlet plane. Experimental data from a series of rig runs have been used to test this CFD deposition modelling approach.

Keywords: Co-firing coal and biomass; particle deposition; vapour deposition; Computational Fluid Dynamics; superheaters and reheaters.

Introduction

Projections of electricity demand show an increase through 2050 as a direct consequence of the economic and efficiency growth [1]. The majority of energy will still be supplied by fossil fuels - mainly natural gas and oil while coal usage will flatten until 2050. The use of renewable will be encouraged, in fact, the exhaustion of natural fossil fuels and the environmental problems related to their use is pushing toward alternative fuels to reduce emissions and increase the boiler efficiency [1]. In this context, biomass is considered one of the most promising sources of renewable energy [2] and co-firing biomass with coal is a valid and cheaper option to reduce CO_2 emissions and increase the energy output without drastic design plant modifications. However, deposit formation onto heat exchangers, also known as fouling and slagging, is one of the major issues during coal and biomass combustion. It can insulate the tube surface reducing the thermal efficiency and lead to tube corrosion which results in high maintenance costs and possibly power plant outages [3].

Deposit formation is the direct consequence of coal and biomass transformation of extraneous and inherent mineral matter during combustion. They release ash particles of different diameters, and vapours of alkali species which can deposit on the tube surface [4]. Vapours can condense homogeneously in the gas phase or heterogeneously on solid particles and on heat exchanger deposit surfaces [4]. Solid ash particles can deposit according to a variety of mechanisms. Inertial impaction is one the main for solid ash particles (d_p > 10 μm) impacting mainly on the upstream sides of tubes as they have enough inertia to overcome the drag force. Smaller particles tend to follow the flue gas streamline and hit the downstream of tubes as a consequence of the eddy impaction (d_p < 10 μm), thermophoresis and Brownian diffusion (d_p < 1 μm) [5]. Thermophoresis and vapour condensation are more significant when the tube surface is clean as they depend on the temperature gradient

between the bulk gas and the surface. However the total deposition rate is enhanced in the presence of a sticky layer of alkali vapours on the tube surface or chemical reactions in the deposit or in the gas phase which can lead to eutectic mixes with lower melting points.

The high variability of fuels, especially biomass, whose properties change with location and climate, makes the deposit formation difficult to predict [6]. Moreover, the multidisciplinary nature of this subject makes its study more complicated and, even though many experimental data and modelling have been carried out so far, the number of gaps in the field is still high. In fact, several studies have been conducted on a lab scale to predict deposit formation which seems to be different compared with industrial scale. Moreover, many indices and mechanistic models have been developed in the literature to predict deposition [7], but they are specific for certain boilers and fuels and cannot be generalized. In addition to that, they are not able to predict the most critical areas where fouling and slagging occur and the dynamic effect of deposit accumulation on heat transfer [8]. For such a complex and multidisciplinary subject, computational fluid dynamics (CFD) has been recognized as one of the best tools to study deposition onto heat exchangers as it allows calculation of both gas and particle behaviour, including deposition flux and modelling mass and heat transfer. However, this modelling approach needs more studies to include the combination of different deposition mechanisms, and validation of the model with experimental data generated by the use of coal and biomass [9,10].

In previous works, the deposition has been studied according to several sticking criteria based on the physical properties of particles and surfaces. Waclawiak et al. [11,12] studied a model for “powdery “ deposit which is more suitable when a dry particle hits a clean surface in low temperature regions. In this case, the deposition is due to a force balance that involves the particle and tube material properties, Van der Waals force and the gravity force. Moreover, “bonded” deposits, made from sticky or molten/semimolten ash particles, were predicted with sticking probability correlations based on the ash particle softening temperature or viscosity [13]. Yang et al. [14] took into account the sticking/rebounding particle behaviour after the impaction on tubes with an energy conservation analysis which includes the ash chemistry, particle and surface properties and furnace operating conditions. However, only a limited number of studies have investigated the vapour condensation contribution and one of the common issues was the prediction of material properties and constants used in the model equations.

The main objective of this paper was to study the deposition on air cooled probes during the combustion of Miscanthus and Daw Mill coal in a 100 kWth pulverized pilot scale combustion test rig at Cranfield University. Ash particle analyses were carried out using Environmental Scanning Electron Microscope (ESEM) and a Malvern Mastersizer 2000 Laser Diffraction instrument for ash particle size distribution. A CFD model was developed in Fluent® combined with User Defined Functions (i.e. UDFs) to predict deposit growth on heat exchangers. This allowed a combination of different deposition mechanisms to be included which could also take into account the stickiness of the particle and the surfaces. Experimental data were used to implement the model boundary conditions and generate results for the model validation.

2. Experimental procedure

2.1 Fuels

The fuels used for this study were Daw Mill Coal and Miscanthus, both provided by E.ON Engineering plc (Technology Centre, Ratcliffe-on-Soar, Nottingham, UK). The proximate, ultimate and ash analyses of both fuels are shown in Table 1. Miscanthus has a higher moisture content and a lower calorific value when compared with Daw Mill Coal. Ultimate analysis of the fuels shows that Miscanthus has a lower carbon, sulphur and chlorine content but higher oxygen content than Daw Mill Coal. The fuels were pulverized and a blend of 12 wt.% Miscanthus balance Daw Mill Coal was used for the following study with an average fuel feed rate of about 8 kg/hr.

Table 1: Daw Mill and Miscanthus characterization (wt. %) on as received basis.

	Daw Mill Coal	Miscanthus
Proximate analysis (wt % AR)		
Moisture	3.20	40.00
Ash content	12.39	2.85
Volatile matter	27.59	-
Calorific value (kJ/kg)		
Gross calorific value	25,300	9,740
Net calorific value	26,290	11,440
Ultimate analysis (wt % AR)		
Carbon	67.08	28.75
Hydrogen	4.16	3.30
Nitrogen	1.16	0.33
Oxygen	10.32	24.60
Sulphur	1.43	0.07
Chlorine	0.23	0.11
Fluorine	0.02	-
Ash composiiton (wt % of total ash)		
SiO_2	36.80	63.00
Al_2O_3	23. 90	0.45
Fe_2O_3	11.20	0.36
TiO_2	1.10	-
CaO	12.00	7.10

MgO	2.50	2.85
Na_2O	1.50	0.18
K_2O	0.50	14.80
Mn_3O_4	0.40	-
P_2O_5	<0.30	1.75
SO_3	12.90	3.70
BaO	-	-

2.2 Pilot scale combustor test facility

The tests were carried out in a 100 kWth capacity downward firing pulverized fuel (PF) pilot-scale combustion rig at Cranfield University (Fig. 1). The rig was heated up with natural gas before switching to pulverized fuels. A multi-fuel excess air burner was used to ensure complete combustion. The fuel was fed to the burner from a hopper using a pneumatic system and a nitrogen flow of 30 L/min. This system incorporated a shaker to prevent the fuels from slumping and agglomerating. The rig worked at negative pressure to avoid the gas escaping into the laboratory and a more detailed description of it is given in [15].

Annular air-cooled ceramic probes were located in the vertical section of the combustor for the deposition study (as highlighted in Fig. 1 (left) and shown in Fig. 1 (right)). The ceramic was mullite, an aluminosilicate similar to the deposit surfaces in real power plants. The flue gas had a velocity of ~ 1.9 m/s, calculated considering the combustion section (300x300 mm) and the air flow rate (2450 L/min) at ~ 1273 K. Temperatures were recorded at different sections along the combustor with R type thermocouples, and K type thermocouples were used to monitor the ceramic probe temperature. Moreover, a multi –component Fourier Transform Infra-Red (FTIR) gas analyser was used to detect the main flue gas components (CO_2, O_2, H_2O, SO_2, CO, NO, N_2O, HCl). During the test runs, the fuel feed rate was adjusted (7 - 9 kg/hr) to keep the oxygen concentration about 4%vol.

Some of the experimental data (gas velocity and temperature, ash composition and ash particle size distribution) were used as boundary conditions in the CFD model, some others (e.g. deposition flux) for its validation.

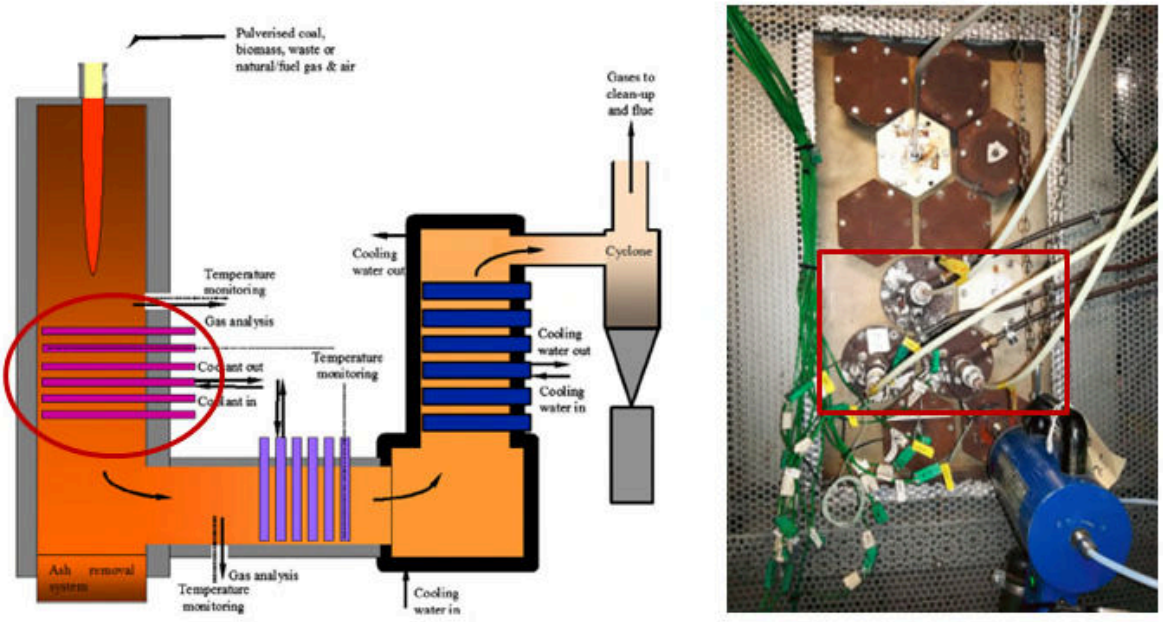

Figure 1: Schematic of the pilot scale pulverized combustion rig (100 kWth) at Cranfield University (left) [16]; detail of the vertical section of the combustor where the deposition probes were located (right)).

2.3 Deposit analysis

In this study, three annular air-cooled ceramic probes (outer diameter, d_t= 39 mm) were used to collect deposits after combustion of pulverized fuels. The compressed air flow rates were adjusted during the tests to keep the probe temperatures at ~500 ˚C in order to simulate real boiler superheaters and reheaters.

The probes were assembled and cleaned with isopropanol before each test and thermocouples were fixed on the probes to record their temperatures. Several view ports were located along the combustor and they were used to check if the fuel was burning properly and to observe the deposit accumulation on some of the probes.

At the end of each test, once the combustor had cooled down with an air flow, the probes were taken out carefully and the deposits were collected from the upstream (top), sidestream (sides) and downstream (bottom) surfaces whose area were previously calculated. Deposit from the different sides of probes was then weighed to calculate the deposition flux. Moreover, some ash samples were collected from the ports where the probes were located (Fig. 1 (right)) and it was assumed that this ash represented the fly ash that caused particle deposition. The samples were analysed to get an ash particle size distribution (conducted at Doosan Babcock - Renfrew, Scotland - using a Malvern Mastersizer 2000) and the results were fitted to the Rosin Rammler model to get parameters needed for the ash distribution required by the Fluent® model [17]. Moreover, ESEM analysis was conducted for all the ash and deposit samples to examine the fly ash and deposit compositions.

3 CFD Modelling

3.1 Geometry and model set up

A CFD approach was chosen to study the fluid dynamics around probes and the deposition behaviour. For this, Fluent® 17.1, enhanced with User Defined Functions (i.e. UDFs), was used to predict deposit growth on three ceramic probes in the Cranfield combustion rig.

The geometry was simplified to a 2D domain to reduce the computational costs linked to the deposition flux calculations, the deposit shape and temperature predictions. The geometry was obtained by a 90˚ rotation anticlockwise (L= 2.45 m, H= 0.30 m) of the combustor in Fig.1, with the bend ~ 0.5 m after the probes being neglected to reduce computational costs. However, it was demonstrated that the presence of the bend does not have a significant influence on the ash particle behaviour and deposition processes on the probes (section 4.2). In Fig.2 the flue gas enters on the left (inlet at 2 m/s and 1273 K), flows across the tubes (outer diameter, d_t = 39 mm, at a constant T_t= 773 K) and leaves the domain at the right boundary condition (pressure outlet). The inlet was placed at $20d_t$ from the first tube and the outlet at $40d_t$ from the last tube to avoid the flow reflection and allow the vortex shedding to be developed enough [18,19].

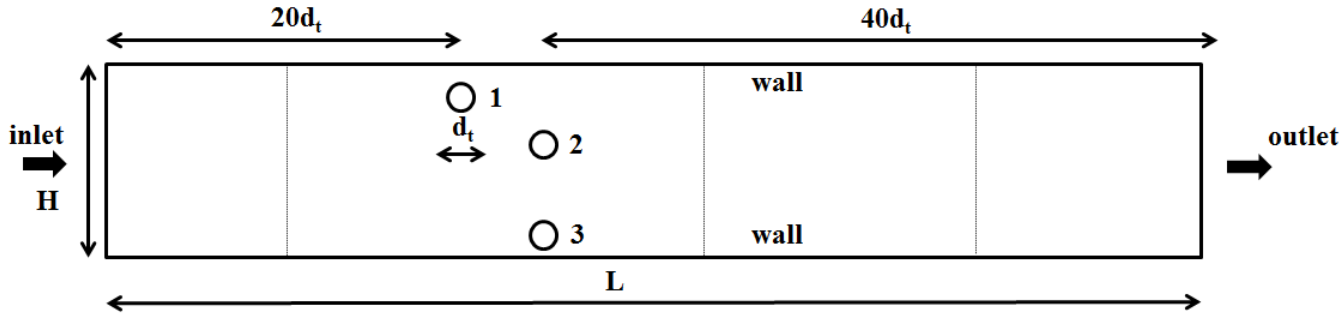

Figure 2: Geometry and boundary conditions.

A grid sensitivity study was carried out to ensure that the results were independent from the grid size and triangular mesh was chosen in order to simulate the deposit shape using DEFINE_GRID_MOTION UDF (which only works with this kind of mesh if the remeshing option is enabled [11,20]). The geometry was divided in four zones using three interiors (vertical lines in Fig.2) as boundary conditions. This is a method used to avoid the degeneration of the mesh when the domain is too big and to make the meshes finer gradually around the tubes (Fig.3).

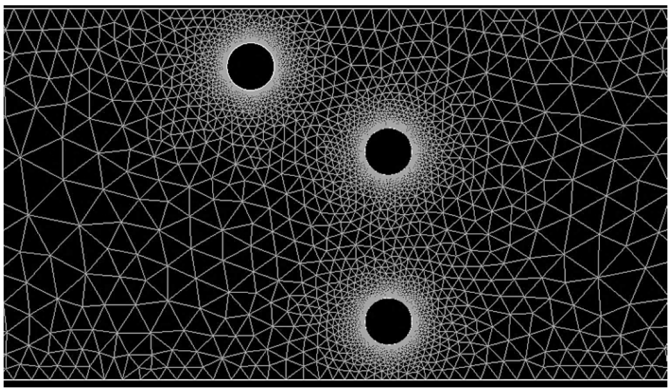

Figure 3 Detail of the triangular mesh around probes.

The flue gas was approximated to be air (ρ_g= 0.345 kg/m^3, Cp_g= 1,146 J/kg K, k_g= 0.069 W/m K, μ_g= 44.07 10^{-6} kg/m s) and ash particles were assumed to be inert (ρ_p= 2200 kg/m^3, Cp_p= 923 J/kg K, k_p= 1.5 W/m K).
The Reynolds number (Re≈ 610) is such that the von Kárman vortex trail is turbulent. Other parameters selected were: the Reynolds Averaged Navier-Stokes (RANS) approach was used for studying the flow and the turbulent model k-ω SST was chosen.

Simulations were run for the fluid without any particles until the flow was developed around the tube, then particles were injected at the inlet surface. The mass flow rate of ash particles (~10^{-4} kg/s) was calculated considering the fuel feed rate and the ash percentage in the fuel.

The dynamic nature of vortex shedding and deposition phenomenon led to a transient approach with a time step size equal to 10^{-3} s which ensures a Courant number < 1. The model was developed using the Discrete Phase Model DPM in Fluent® [21]. The Eulerian model describes the continuous phase and the Lagrangian model is used to describe particle trajectories. The integration of Eq. 1 allows the calculation of ash particle trajectories.

$$\frac{du_p}{dt} = F_D\left(u_g - u_p\right) + \frac{g_x(\rho_p - \rho_g)}{\rho_p} + F_x \qquad (1)$$

where: $F_D\left(u_g - u_p\right)$ is the drag force per unit particle mass; g_x is the gravitational force; F_x the additional force term (e.g. Brownian, Thermophoretic, Lift force etc); u_g is the fluid phase velocity; u_p is the particle velocity; ρ_g is the fluid density; and, ρ_p is the density of the particle. The model took into consideration the force of gravity acting along the moving ash particles with the direction of the flue gas (x positive) and the interaction between the two phases. The dispersion of particles due to the turbulence in the gaseous fluid was included, using the Discrete Random Walk (i.e. DRW) and the Random Eddy Lifetime with time scale constant 0.15 [5,22]. This setting allows

a better prediction of small ash particle behaviour on the downstream. In addition, the thermophoretic force was enabled and the Talbot model was used [23,24].

Inertial impact is recognized as one of the main deposition mechanisms for bigger particles that have more inertia to overcome the drag force and hit the upstream sides of tubes and rebound on neighbour tubes. Small particles instead are more likely to follow the flue gas streamlines, take part of the vortex shedding and hit the lee side [12,25].

3.2 Deposition model

Deposition is a complex and multidisciplinary phenomenon which involves many species and mechanisms [26]. On a clean surface, only vapours and particles that hit the surface in a sticky condition are more likely to deposit [27]. The probability for a particle to sticky depends on the particle and surface properties (i.e., stickiness, roughness), impact angle and particle impaction velocity (Fig. 4).

Deposition represents a major problem in boilers as it creates a resistance between the hot flue gas and the cooling fluid which deeply affects the heat transfer and the thermal efficiency. As a consequence of deposit formation, the temperature of the deposit surface increases and thermophoresis and condensation contributions decrease.

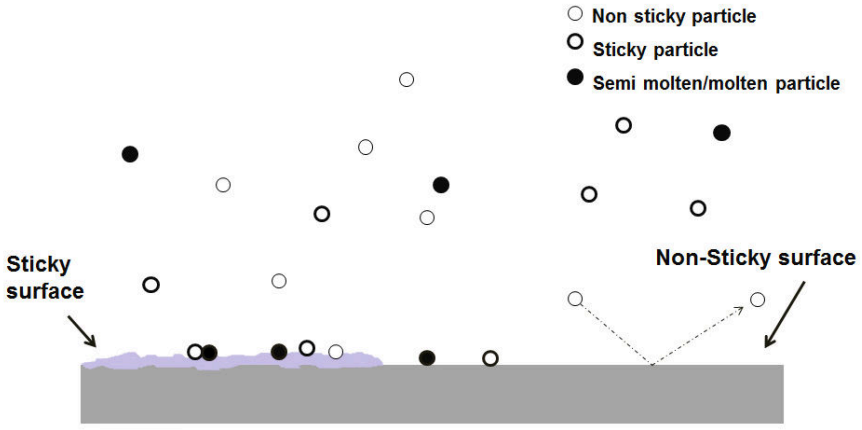

Figure 4: Sticking of particles from a hot gas stream onto a cooled surface.

In this work, deposit accretion was modelled modifying the DEFINE_DPM_EROSION UDF in Fluent® [28]. The deposition flux can be calculated with Eq. 2 as a function of the fouling probability P_f, the mass flow rate m_p of particulate matter striking the deposition surface A and the impaction angle γ (Fig. 5). However, it must be noticed that, in transient simulations, m_p represents only the mass of particles impacting the surface [11]:

$$m_{dep,A} = P_f \frac{dm_p}{dA} sin(\gamma) \qquad (2)$$

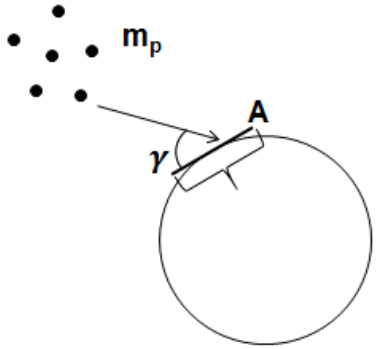

Figure 5: Parameters for particle impaction on tube.

The fouling probability was calculated as a total probability P_{tot}, function of the stickiness of the surface, depending on vapour condensation, and stickiness of the particle which depends on its composition [29,30].

$$P_{tot} = P_w(1 - P_p) + P_p(1 - P_w) + P_w P_p \qquad (3)$$

where: P_w is the wall stickiness probability and P_p is the particle stickiness probability.

For simplicity, Na_2SO_4 1 ppm was considered the only vapour component responsible for condensation and able to create a sticky layer on the tube surface [5].

The probability can be calculated as it follows [5]:

$$P_w = Sm_{c,A} \qquad (4)$$

where the constant *S*, with the inverse dimensions of deposition flux, was experimentally estimated on the basis of the maximum deposit accumulated on the probe during the experiments (~ 24000 $[kg/(m^2\,s)]^{-1}$).

The condensation flux of vapour *i*-th can be calculated using Eq. 5 [5]:

$$m_{c,A,i} = \beta_i \frac{p_i - p_{s,i}}{p} \rho_g \qquad (5)$$

with $m_{c,A,i}$ being the deposition flux and β_i, the mass transfer coefficient of the *i*-th component defined as [31]:

$$\beta_i = ShD_i/d_t \qquad (6)$$

D_i is the diffusion coefficient of the ith component through the flue gases [32], Sh is the dimensionless Sherwood number used in mass-transfer operation, p_i is the partial pressure of *i*-th gaseous component, p is the gas pressure and ρ_g is the gas density.

The saturation pressure of the *i*-th gaseous component at surface temperature, p_{si}, is calculated according to the following formula [5]:

$$\frac{p_{s,i}}{\mathrm{p_n}} = \exp\left(A_i - \frac{B_i}{T + C_i}\right) \qquad (7)$$

where: *A, B* and *C* are given constants in Table 2, $\mathrm{p_n} = 10^5$ Pa and *T* is the tube temperature.

Table 2: Constants A_i, B_i, C_i used in Eq. (7) [5]

Component	A	B	C	T [K]
Na_2SO_4	15.03	37,452.4	0	1,150-1,800
K_2SO_4	18.08	39,449.6	0	1,150-1,800
KCl	11.01	17,132	-122.70	1,094-1,680
NaCl	11.68	19,315	-82.60	1,138-1,738

Moreover, the critical viscosity approach was used to take into account the particle stickiness P_P which was calculated according to the composition *X* and the temperature *T* of the ash particles as follows [30]:

$$P_P(T, X) = \frac{\eta_{ref}}{\eta} \quad \eta > \eta_{ref} \qquad (8)$$

$$1 \quad \eta \leq \eta_{ref} \qquad (9)$$

Following this model, the particle sticking probability is a function of the particle viscosity η and a reference viscosity η_{ref} [33,34]. The particle viscosity was calculated with the ash chemical composition, previously obtained by the ESEM analysis, and temperature of the particles using the model of Urbain [35,36], where $\eta_{ref} = 10^4$ Pa s.

The deposition rate in Eq. 2 considered only the contribution of ash particles; therefore, the total deposition flux was calculated adding also the vapour condensation flux (Eq. 10).

$$m_{tot} = P_{tot} \frac{dm_p}{dA} sin(\gamma) + m_{c,A} \qquad (10)$$

3.3 Grid motion

The shape of the deposit was simulated by applying DEFINE_GRID_MOTION UDF to the probe surface in the CFD model. The deposition flux calculated in DEFINE_DPM_EROSION can be used to estimate the deposit thickness δ_j at each node *j* taking into account the deposit density ρ_{dep} and the time [37].

The accretion direction was obtained calculating the angle θ normal to each face defined as in Eq. (11) and Fig. 6:

$$\theta = \tan^{-1}(Y_P/X_P) \qquad (11)$$

The new coordinates of the nodes at different locations around the probe were determined with Equations 12 and 13.

$$X'_p = X_p + \delta_j \cos\theta \qquad (12)$$

$$Y'_p = Y_p + \delta_j \sin\theta \qquad (13)$$

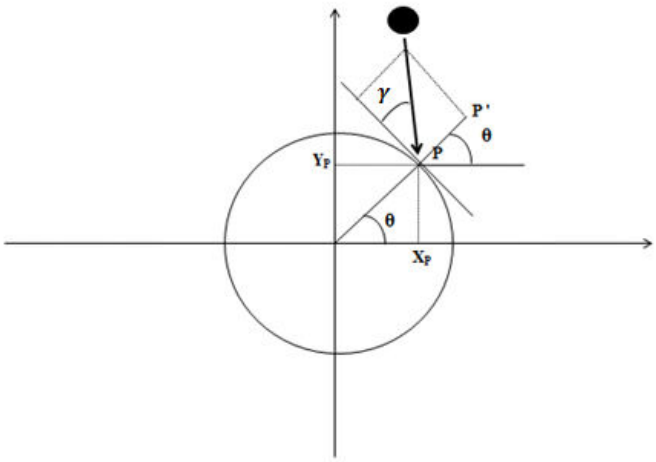

Figure 6: Calculation of new node coordinates.

3.4 Deposit temperature:

The deposit layer formed during the combustion of coal and biomass represents an additional resistance to the heat transfer between the hot flue gas and the cooling fluid (Fig. 7) (ρ_{dep}= 600 kg/m^3, k_{dep}= 3 W/m K, ε_{dep} = 0.7) [13,38,39]. Therefore, the surface temperature of the deposit ($T_{5,S}$) tends to increase with the deposit thickness and this reduces one of the driving forces related to vapour condensation and thermophoresis (gas-surface temperature differences) [39].

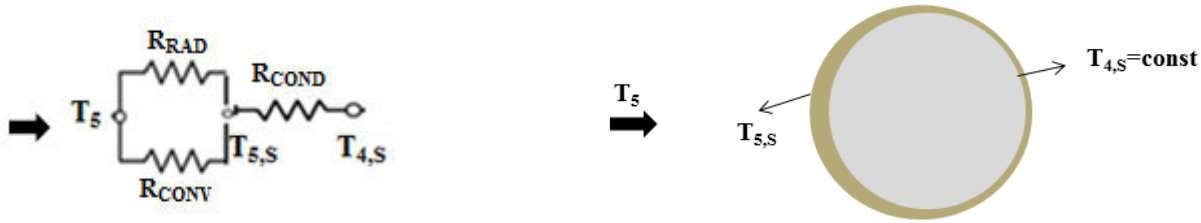

Figure 7: Effect of deposit build up on the surface temperature.

In this work, the deposit temperature was calculated using DEFINE_PROFILE UDF where Equations 14 and 15 were implemented and the deposit thickness δ_i was obtained from DEFINE_DPM_EROSION UDF. The ceramic probe surface temperature was assumed to be constant ($T_{4,S}$= 773 K) and the deposit temperature was calculated considering the external heat flux $\dot{q}_{tot}$ due to the radiation and convection and the deposit thermal resistance R, function of the deposit thickness δ_i and thermal conductivity k_{dep}.

$$T_{5,S} = \dot{q}_{tot}\, R + T_{4,S} \qquad (14)$$

$$R = \frac{\delta_i}{k_{dep}} \qquad (15)$$

4 Results and discussion

4.1 Deposit characterization

Deposits were collected at the end of tests of 2.5 and 5 hours respectively (Fig. 8). Thicker deposits were found on the top of each probe where, the main deposition mechanism for bigger particles is the inertial impact. Generally, deposits looked quite powdery and sand color, thicker on the top than on the side and bottom. Despite possible ash loss while taking the probes out, the deposition fluxes for both tests were comparable. The thickness of the deposit accumulated after 2.5 hours (Fig. 8 (left)) was smaller than after 5 hours (Fig. 8 (right)) with a maximum thickness on the upstream of ~ 0.5 cm and ~ 1 cm respectively. It was more difficult to measure it on the sides and downstream where a very thin layer of ash was found, more powdery on the sidestream and stickier on the bottom where vapour condensation is more likely to occur.

Figure 8: Deposits after 2.5 hours (left) and 5 hours (right) of exposure.

Deposit was brushed off and collected from the upstream, sidestream and bottom surfaces. Once weighed, the deposition flux was calculated taking into account the area of each part of the tube and the exposure duration. As expected, the deposition flux (Fig. 14 (left)) was higher on the top than on the side and bottom. Probes 1 and 3

showed slightly higher values and this could be due to the presence of the furnace wall which increases the number of particle bounds and rebounds.

The ESEM analysis was conducted for all the samples, images were captured from the different sides (Fig. 9) and the ash composition was calculated based on the main oxides. Ash is mainly made up of aluminosilicates, however the results of chemical ash analysis are generally expressed in terms of weight % of their highest oxides and the main components using this convention are presented as SiO_2, Al_2O_3, Fe_2O_3 (Fig. 10).

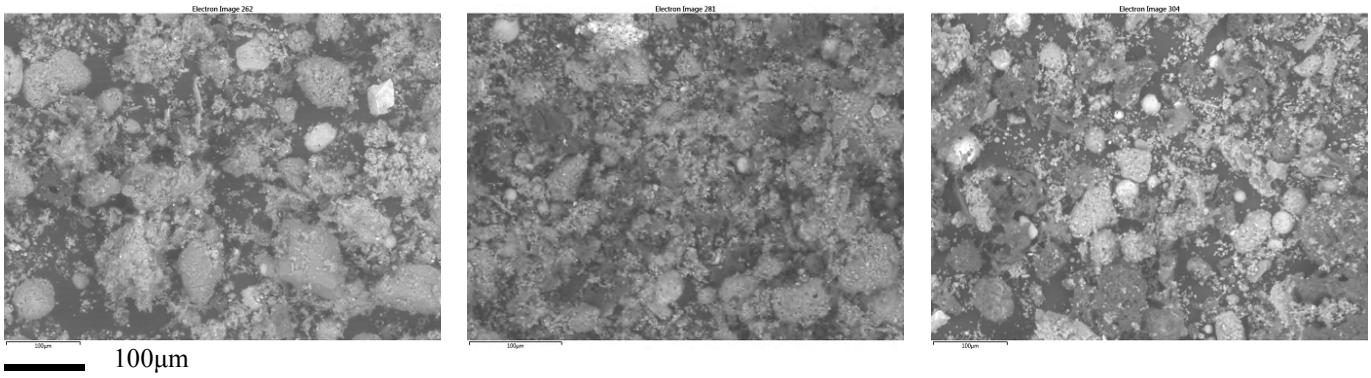

Figure 9: SEM images of deposit on different probe locations.

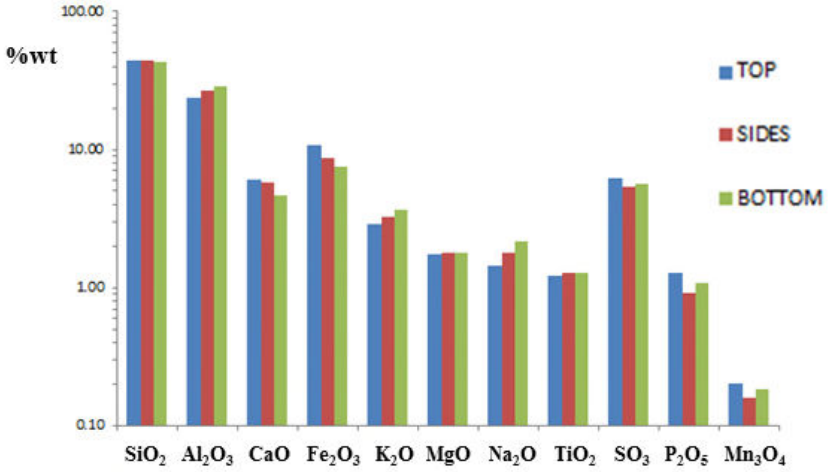

Figure 10: Fly ash composition.

An ash particle size distribution was obtained from laser diffraction analysis (carried out by Doosan Babcock) with a Malvern Mastersizer 2000 (Fig. 11). The volumetric distribution was used to calculate a cumulative particle size distribution with the Rosin Rammler model and the main parameters were: d_{min}= 0.43 µm, d_{max}= 535 µm, d_{mean}= 68 µm, n= 1.07.

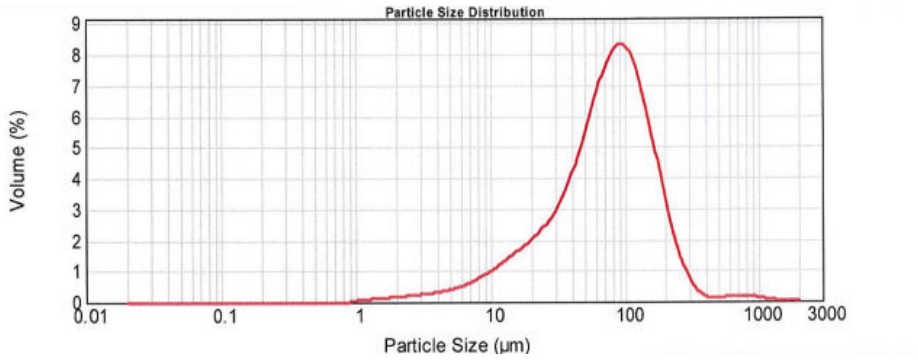

Figure 11: Fly ash particle size distribution.

4.2 Model prediction

A predictive CFD model has been developed using Fluent® with UDFs for ash and vapour deposition on ceramic probes in a pilot scale combustion rig at Cranfield. The mesh in Fig. 3 was implemented with the relative boundary conditions, material properties and turbulence model. The flue gas was studied without particles until at least a partial convergence was reached. The Discrete Phase Model was then enabled with interaction between gas and solid phases and the ash particle trajectories (Fig. 12) were obtained implementing the Rosin Rammler particle size distribution from Fig. 11. Bigger particles tend to hit the front of the tube, smaller particles are more likely to follow the flue gas streamline and deposit on the sidestream and downstram. However, the presence of the furnace walls and the neighboring probes can increase the bound and rebound frequency from one tube to the other. This can be noticed by a higher concentration of bigger particles (red) on the downstream of probe 1 that may be due to the particle rebounding from the top side of probe 2 (Fig. 12).

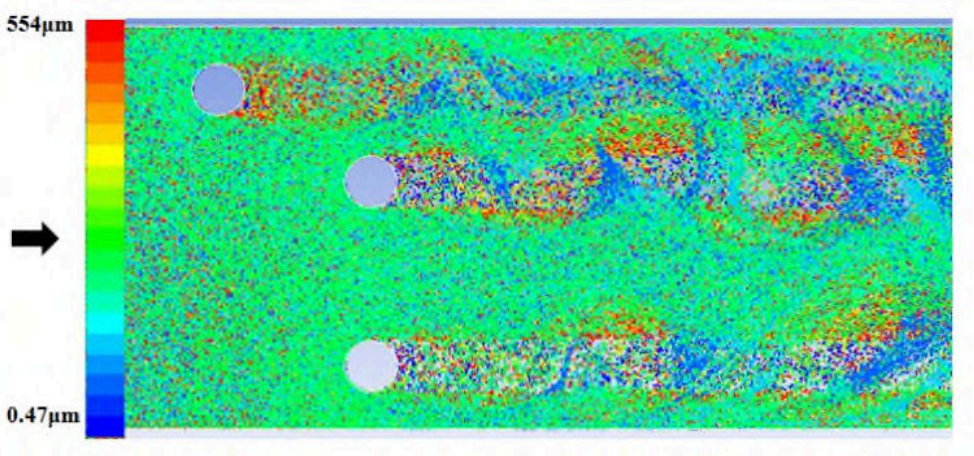

Figure 12: Ash particle trajectories (d_{min}= 0.43 µm, d_{max}= 535 µm, d_{mean}= 68 µm, n= 1.07).

Deposition was studied using DEFINE_DPM_EROSION UDF including the total stickiness of particles and vapour condensation. The probability for a particle to deposit is higher on a sticky surface or if the particle is

sticky, molten or semimolten because of previous chemical reactions. This effect was captured from one of the view ports during a test (Fig. 13).

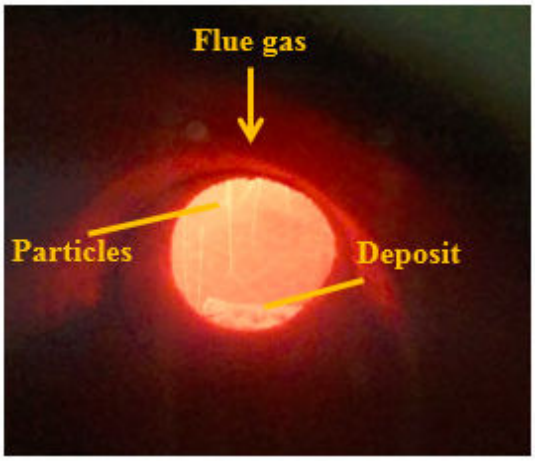

Figure 13: Deposit probe during test.

The fly ash composition, previously calculated with the ESEM analysis, was used to predict the particle stickiness with the Urbain model using Kalmanovitch's modifications [40], and the vapour condensation was included to evaluate the surface stickiness. This latter contributes to the formation of an initial layer, generally sticky, which is able to enhance the particle deposition. In this study, the percentage of ash particles deposited for previous alkali vapour condensation on a probe surface at 773 K was ~ 0.02% of the total deposition flux, but this value is expected to decrease with an increase of the deposit surface temperature. As a consequence, inertial impaction has been demonstrated to be one of the main mechanisms responsible for deposition on the air-cooled ceramic probe surfaces. These results confirm previous findings which demonstrated that the condensation of vapours enhanced the deposition of larger ash particles and is more significant in the early stages of exposures of cooler probe surfaces. However, the proportion of condensed vapour phase species was found to be insignificant when compared with the total deposition flux [4,27,30,41,42].

Simulations were able to correctly predict the deposition location around probes with higher amount of deposit on the upstream surfaces than sidestream and downstream (Fig. 14 (right)). The model seems to overestimate the deposition on the tops and underestimate those on the bottom of the probes. However, this can be explained by the uncertainty linked to the experimental measurements and by the numerical uncertainties associated with the predictions, which include: 2D geometry approximation, the particle sticking models and the deposit properties used in the current paper.

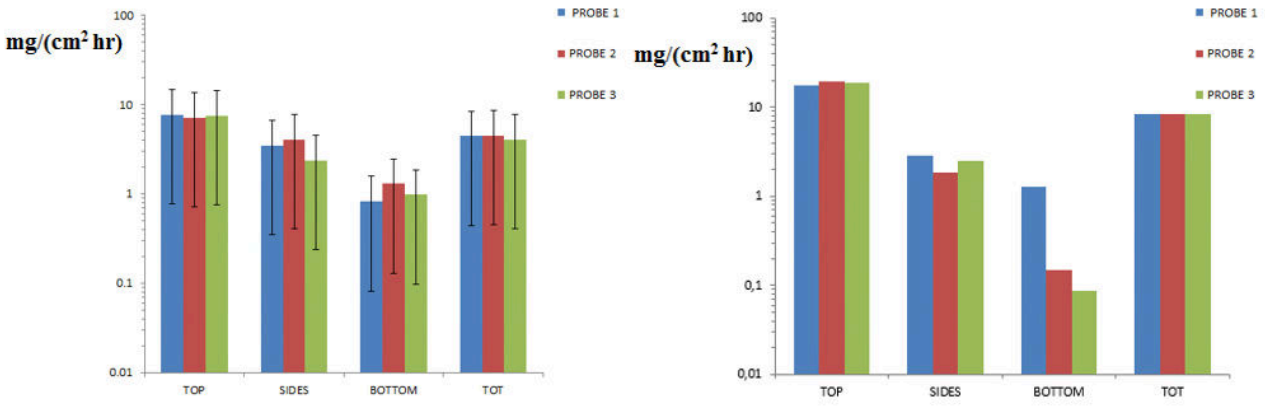

Figure 14: Deposition fluxes from experiments (left) and modelling (right).

Fig. 15 compares the results of deposition flux predictions using the current model (with and without the bend) with the "powdery" model used by Waclawiak et al. [11] and the model used by Yang et al. [14]. Previous values from the literature were used to overcome the difficulties in defining the constants and material properties (e.g. deposit surface tension, contact angle, etc. [14]) in the equations.

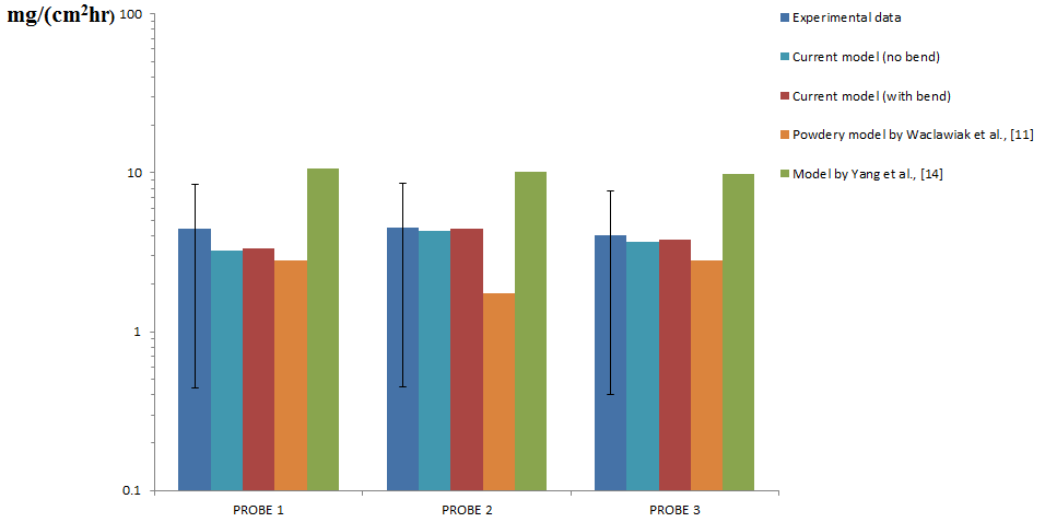

Figure 15: Comparison of the deposition fluxes between the experiments and several sticking models.

The results show that the presence of the bend does not affect the deposition flux on the ceramic probes; therefore the following simulations used the straight geometry which implies less computational costs. Moreover, the powdery deposit [11] tends to underestimate the experimental values, while the model developed by Yang et al. [14] overestimates the experimental deposition flux. However, this latter model is generally used to predict slagging at high temperatures, rather than fouling in convective areas and it was applied using the soda-lime glass

properties defined in Yang et al. [14]. Therefore, future studies may include an investigation of the deposit properties to improve the quality and reliability of new model predictions.

The shape of the deposit was predicted after 2.5 hours and 5 hours using Equations 12 and 13. As expected, the deposit looks thicker after 5 hours and only a very thin layer was found on the downstream (Fig. 16), as shown also in the experimental results (Figures 8).

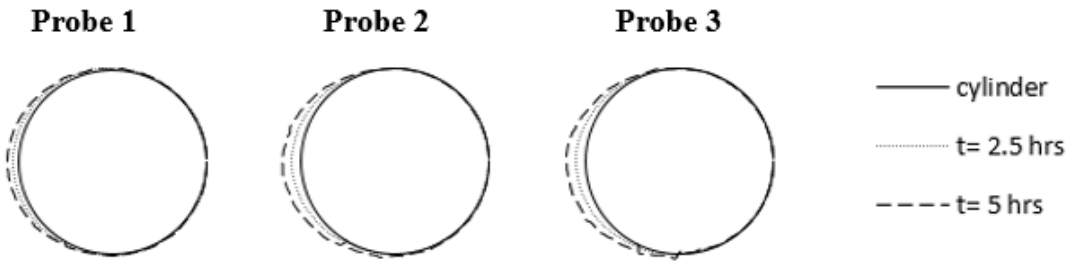

Figure 16: Deposit shape after 2.5 and 5 hours of exposure.

Predictions of deposit surface temperature after 2.5 and 5 hours of exposure are reported in Fig. 17 as function of the angle described around probe 1. In agreement with previous results from literature, deposit accumulation affects the thermal resistance R which leads to increasing deposit temperature; the highest temperature was identified at the upstream, followed by the sidestream and downstream.

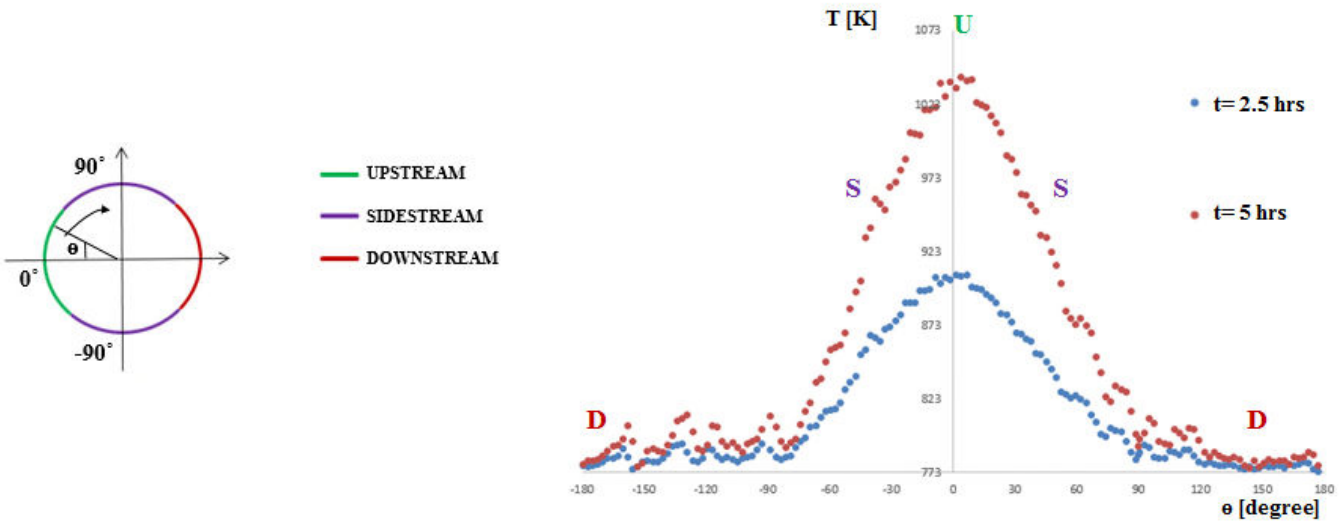

Figure 17: Illustration of probe sides (left); deposit temperature after 2.5 and 5 hours of exposure (right).

Conclusions

In this work, a CFD model has been developed for deposit prediction on ceramic probes in a 100 kWth pilot scale combustion rig at Cranfield University. This model has been validated using data from the operation of

this rig using pulverized coal and biomass fuels. Fluent®, enhanced with UDFs, was the software used to simulate the deposit accumulation as well as its shape and surface temperature. The ash obtained during the combustion of Daw Mill Coal and Miscanthus was analysed to get the chemical composition and ash particle size distribution. These data were then used as boundary conditions in the model and predictions of the deposition flux were compared to the experimental results. In this work, the geometry was simplified to a 2D domain and an Eulerian Lagrangian approach was used to simulate the gas and ash particle behaviour around the probes.

The deposition flux was calculated using a modification of the DEFINE_DPM_EROSION UDF where the stickiness of particles and surface were both taken into account. In addition, the results of these calculations were used to predict deposit shapes and thicknesses using a modification of the DEFINE_GRID_MOTION UDF procedure and the deposit surface temperature with DEFINE_PROFILE.

Future studies will be carried out to optimize the model with further experimental results and include the effect of a dynamic shape and surface temperature on the deposition flux.

Acknowledgments

The authors acknowledge the support of the Engineering and Physical Research Council (EPSRC) for their support for the project - Flexible and Efficient Power Plant: Flex-E-Plant (Grant number: EP/K021095/1). They also thank the following partners for their valuable contributions: GE Power, Doosan Babcock Limited, Centrica plc., EDF Energy (West Burton Power) Limited., Uniper Technologies Limited, Goodwin Steel Castings Limited, NPL Management Limited, R-MC Power Recovery Limited., RWE Generation UK plc., Scottish and Southern Energy (SSE) plc., Siemens Industrial Turbomachinery, and TWI Limited.

References

1. U.S. Energy Information Administration. Annual Energy Outlook. 2018. Available at: DOI:DOE/EIA-0383(2017)
2. Mckendry P. Energy production from biomass (part 1): overview of biomass. Bioresource Technology. 2002; 83: 37–46.
3. Nunes LJR., Matias JCO., Catalão JPS. Biomass combustion systems : A review on the physical and chemical properties of the ashes. Renewable and Sustainable Energy Reviews. Elsevier; 2016; 53: 235–242. Available at: DOI:10.1016/j.rser.2015.08.053

4. Schulze K., Scharler DR., Telian DIM. Advanced modelling of deposit formation in biomass furnaces – investigation of mechanisms and comparison with deposit measurements in a small-scale pellet boiler. Impacts of fuel quality. 2010; : 1–14.
5. Tomeczek J., Wacławiak K. Two-dimensional modelling of deposits formation on platen superheaters in pulverized coal boilers Flue gas. Fuel. Elsevier Ltd; 2009; 88(8): 1466–1471. Available at: DOI:10.1016/j.fuel.2009.02.023
6. Pisa I., Lazaroiu G. Influence of co-combustion of coal/biomass on the corrosion. Fuel Processing Technology. 2012; 104: 356–364. Available at: DOI:10.1016/j.fuproc.2012.06.009
7. Borio RW., Levasseur AA. Overview of Coal Ash Deposition in Boilers. Combustion Engineering. 1984; 29(4): 193–203.
8. Magda A., Magda SI., Strelow M., Muller H., Leithner R. CFD modelling of ash deposits in coal-fired power plants. Heat Exchanger Fouling and Cleaning. 2011. pp. 301–308.
9. Weber R., Mancini M., Schaffel-mancini N., Kupka T. On predicting the ash behaviour using Computational Fluid Dynamics. Fuel Processing Technology. Elsevier B.V.; 2013; 105: 113–128. Available at: DOI:10.1016/j.fuproc.2011.09.008
10. Magda A. Modelling of Mineral Matter Transformation and Deposition in Furnaces. 2012.
11. Wacławiak K., Kalisz S. Using Fluent code to predict deposition during combustion of solid fuels. Heat Exchanger Fouling and Cleaning. 2011. pp. 294–300.
12. Wacławiak K., Kalisz S. A practical numerical approach for prediction of particulate fouling in PC boilers. Fuel. 2012; 97(97): 38–48. Available at: DOI:10.1016/j.fuel.2012.02.007
13. Kleinhans U., Wieland C., Frandsen FJ., Spliethoff H. Ash formation and deposition in coal and biomass fired combustion systems: Progress and challenges in the field of ash particle sticking and rebound behavior. Progress in Energy and Combustion Science. Elsevier Ltd; 2018; 68: 65–168. Available at: DOI:10.1016/j.pecs.2018.02.001
14. Yang X., Ingham D., Ma L., Troiano M., Pourkashanian M. Prediction of particle sticking efficiency for fly ash deposition at high temperatures. Proceedings of the Combustion Institute. Elsevier Inc.; 2018. pp. 1–9. Available at: DOI:10.1016/j.proci.2018.06.038
15. Khodier A. Co-firing fossil fuels and biomass: combustion, deposition and modelling. Cranfield University;

2011.

16. Hussain T., Khodier AHM., Simms NJ. Co-combustion of cereal co-product (CCP) with a UK coal (Daw Mill): Combustion gas composition and deposition. Fuel. Elsevier Ltd; 2013; 112: 572–583. Available at: DOI:10.1016/j.fuel.2013.01.001

17. Bailey AG., Balachandran W., Williams TJ. The Rosin-Rammler size distribution for liquid droplet ensembles. Aerosol Science. 1983; 14(1): 39–46.

18. Dröge MT. Chapter 5 Flow Around a Circular Cylinder. University of Groningen Cartesian; 2007.

19. Rahman MM., Karim MM., Alim MA. Numerical investigation of unsteady flow past a circular cylinder using 2-D finite volume method. Journal of Naval Architecture and Marine Engineering. 2008; 4(1). Available at: DOI:10.3329/jname.v4i1.914

20. García Pérez M., Vakkilainen E., Hyppänen T. Unsteady CFD analysis of kraft recovery boiler fly-ash trajectories, sticking efficiencies and deposition rates with a mechanistic particle rebound-stick model. Fuel. 2016; 181(181): 408–420. Available at: DOI:10.1016/j.fuel.2016.05.004

21. Hosseini SB., Khoshkhoo RH., Malabad SMJ. Numerical study on polydisperse particle deposition in a compact heat exchanger. Applied Thermal Engineering. Elsevier Ltd; 2017; 127: 330–346. Available at: DOI:10.1016/j.applthermaleng.2017.08.023

22. Lee B., Hwang M., Seon C., Jeon C. Numerical prediction of characteristics of ash deposition in heavy fuel oil heat recovery steam generator †. Journal of Mechanical Science and Technology. 2014; 28(7): 2889–2900. Available at: DOI:10.1007/s12206-014-0643-z

23. Fluent. Discrete Phase Models. FLUENT User's Guide. 2001. pp. 1–170. Available at: http://www.afs.enea.it/fluent/Public/Fluent-Doc/PDF/chp19.pdf

24. Talbot L. Thermophoresis of particles in a heated boundary layer. Fluid Mechanics. 1980; 101(4): 737–758.

25. Baxter L. Ash deposition during biomass and coal combustion: a mechanistic approach. Biomass and Bioenergy. 1993; 4(2): 85–102.

26. Khodier AHM., Hussain T., Simms NJ., Oakey JE., Kilgallon PJ. Deposit formation and emissions from co-firing miscanthus with Daw Mill coal : Pilot plant experiments. Fuel. Elsevier Ltd; 2012; 101: 53–61. Available at: DOI:10.1016/j.fuel.2011.09.029

27. Zhou H., Jensen PA., Frandsen FJ. Dynamic mechanistic model of superheater deposit growth and shedding

in a biomass fired grate boiler. Fuel. 2007; 86: 1519–1533. Available at: DOI:10.1016/j.fuel.2006.10.026

28. ANSYS FLUENT. ANSYS FLUENT 12.0 UDF Manual. 2009.

29. Schulze K., Scharler R., Obernberger I. Development of an advanced CFD model for ash deposit and aerosol formation in biomass fired boilers. 9th European Conference on Industrial Furnaces and Boilers. 2011. pp. 1–11.

30. Kær SK., Rosendahl LA., Baxter LL. Towards a CFD-based mechanistic deposit formation model for straw-fired boilers. Fuel. 2006; 85: 833–848. Available at: DOI:10.1016/j.fuel.2005.08.016

31. Incropera FO. Fundamentals of heat and mass transfer. 2006.

32. Green DW., Perry RH. Perry's Chemical Engineer's Handbook. 2008.

33. Richards GH., Slater PN., Harb JN. Simulation of Ash Deposit Growth in a Pulverized coal fired pilot scale reactor. Energy & Fuel. 1993; 7: 774–781.

34. Walsh PM., Sayre AN., Loehden DO., Monroe LS., Beer JM., Sarofim AF. Deposition of bituminous coal ash on an isolated heat exchanger tube: effects of coal properties on deposit growth. Energy Combustion Science. 1990; 16: 327–346.

35. Senior CL., Srinivasachar S. Viscosity of Ash Particles in Combustion Systems for Prediction of Particle Sticking. Energy & Fuel. 1995; 9: 277–283. Available at: DOI:10.1021/ef00050a010

36. Wieland C., Kreutzkam B., Balan G., Spliethoff H. Evaluation , comparison and validation of deposition criteria for numerical simulation of slagging. Applied Energy. Elsevier Ltd; 2012; 93: 184–192. Available at: DOI:10.1016/j.apenergy.2011.12.081

37. García Pérez M., Vakkilainen E., Hyppänen T. 2D dynamic mesh model for deposit shape prediction in boiler banks of recovery boilers with different tube spacing arrangements. 10th International Conference on Heat Transfer, Fluid Mechanics and Thermodynamics. 2014. pp. 1162–1171.

38. García Pérez M. Modeling the effects of unsteady flow patterns on the fireside ash fouling in tube arrays of kraft and coal-fired boilers. Lappeenranta University of Technology; 2016.

39. Furmański P. Thermal and radiative properies of ash deposits on heat transfer surface of boilers. Warsaw; 1995.

40. Browning GJ., Bryant GW., Hurst HJ., Lucas JA., Wall TF. An empirical method for the prediction of coal ash slag viscosity. Energy and Fuels. 2003; 17(3): 731–737. Available at: DOI:10.1021/ef020165o

41. Leppänen A., Tran H., Taipale R., Välimäki E., Oksanen A. Numerical modeling of fine particle and deposit formation in a recovery boiler. Fuel. 2014; 129: 45–53. Available at: DOI:10.1016/j.fuel.2014.03.046

42. Yang X., Ingham D., Ma L., Zhou H., Pourkashanian M. Understanding the ash deposition formation in Zhundong lignite combustion through dynamic CFD modelling analysis. Fuel. 2017; 194: 533–543. Available at: DOI:10.1016/j.fuel.2017.01.026

2019-05-27

Deposition prediction in a pilot scale pulverized fuel-fired combustor

Chiara, Riccio

Elsevier

Riccio C, Simms NJ, Oakey JE. (2019) Deposition prediction in a pilot scale pulverized fuel-fired combustor. Fuel, Volume 253, October 2019, pp.1204-1213
https://doi.org/10.1016/j.fuel.2019.05.077